

SDSSJ143244.91+301435.3: a link between radio-loud narrow-line Seyfert 1 galaxies and compact steep-spectrum radio sources?

A. Caccianiga¹, S. Antón^{2,3}, L. Ballo¹, D. Dallacasa^{4,8}, R. Della Ceca¹, R. Fanali⁵, L. Foschini¹, T. Hamilton⁶, A. Kraus⁷, T. Maccacaro¹, K.-H. Mack⁸, M.J. Marchã⁹, A. Paulino-Afonso², E. Sani¹⁰, P. Severgnini¹

¹INAF - Osservatorio Astronomico di Brera, via Brera 28, I-20121 Milan, Italy

²Faculdade de Ciências da Universidade de Lisboa, Campo Grande, P-1749-016 Lisboa, Portugal

³Instituto de Astrofísica de Andalucía - CSIC, PO Box 3004, 18008 Granada, Spain

⁴Dipartimento di Astronomia, Università di Bologna, via Ranzani 1, 40127, Bologna, Italy

⁵Dipartimento di Fisica G. Occhialini, Università di Milano-Bicocca, Piazza della Scienza 3, 20126, Milano, Italy

⁶Department of Natural Sciences, Shawnee State University, 940 2nd Street, Portsmouth, OH 45662, USA

⁷Max-Planck-Institut für Radioastronomie, Auf dem Hügel 69, D-53121 Bonn, Germany

⁸INAF - Istituto di Radioastronomia, Via Gobetti 101, I-40129 Bologna, Italy

⁹32 Ordnance Hill, London NW8 6PU, UK

¹⁰INAF - Osservatorio Astrofisico di Arcetri, Largo E. Fermi 5, 50125, Firenze, Italy

ABSTRACT

We present SDSSJ143244.91+301435.3, a new case of radio-loud narrow line Seyfert 1 (RL NLS1) with a relatively high radio power ($P_{1.4GHz}=2.1\times 10^{25}$ W Hz⁻¹) and large radio-loudness parameter ($R_{1.4}=600\pm 100$). The radio source is compact with a linear size below ~ 1.4 kpc but, contrary to most of the RL NLS1 discovered so far with such a high $R_{1.4}$, its radio spectrum is very steep ($\alpha=0.93$, $S_\nu \propto \nu^{-\alpha}$) and not supporting a “blazar-like” nature. Both the small mass of the central super-massive black-hole and the high accretion rate relative to the Eddington limit estimated for this object ($3.2\times 10^7 M_\odot$ and 0.27, respectively, with a formal error of ~ 0.4 dex on both quantities) are typical of the class of NLS1. Through a modelling of the spectral energy distribution of the source we have found that the galaxy hosting SDSSJ143244.91+301435.3 is undergoing a quite intense star-formation ($SFR=50 M_\odot y^{-1}$) which, however, is expected to contribute only marginally (~ 1 per cent) to the observed radio emission. The radio properties of SDSSJ143244.91+301435.3 are remarkably similar to those of compact steep spectrum (CSS) radio sources, a class of AGN mostly composed by young radio galaxies. This may suggest a direct link between these two classes of AGN, with the CSS sources possibly representing the misaligned version (the so-called “parent population”) of RL NLS1 showing blazar characteristics.

Key words: galaxies: active - galaxies: nuclei - quasars: individual: SDSSJ143244.91+301435.3

1 INTRODUCTION

Narrow-line Seyfert 1 (NLS1) galaxies have been identified as a peculiar sub-class of AGN on the basis of their relatively narrow (≤ 2000 km s⁻¹) Balmer lines, relatively weak [OIII] $\lambda 5007\text{\AA}$ emission compared to the Balmer lines ($[\text{OIII}]\lambda 5007\text{\AA}/H\beta < 3$) and strong optical FeII (Osterbrock & Pogge 1985; Goodrich 1989; Pogge 2000, 2011; Véron-Cetty, Véron & Gonçalves 2001). The presence of strong iron emission and the low [OIII] $\lambda 5007\text{\AA}/H\beta$ flux ratio suggest that NLS1 are not obscured objects like type 2 AGN, where the observed narrow emission lines are produced in regions (the Narrow Line Region, NLR) that are located far from

the nucleus. In NLS1, instead, the observed Balmer lines are likely produced in the Broad Line Region (BLR) clouds that are located close (< 0.1 pc) the accreting super-massive black-hole (SMBH). If the BLR traces the potential well of the central SMBH, a low velocity dispersion is the result of a combination of a relatively small SMBH mass with a high accretion rate, close to the Eddington limit (L_{Edd}). Indeed, NLS1 are usually characterized by SMBH masses between 10^5 and $10^8 M_\odot$ and accretion rates larger than $\sim 0.1 L_{Edd}$ (e.g. Marziani et al. 2001; Boroson 2002; Greene & Ho 2004; Collin & Kawaguchi 2004; Grupe 2004; Botte et al. 2004; Grupe & Mathur 2004; Zhou et al. 2006; Whalen et al. 2006;

Komossa et al. 2006; Yuan et al. 2008 but see also Decarli et al. 2008; Marconi et al. 2008; Calderone et al. 2013).

An interesting characteristic of NLS1 is their preference of being radio-quiet (RQ) AGN. To date, only ~ 50 radio-loud (RL) NLS1 have been discovered (Foschini 2011). Komossa et al. (2006) has computed the fraction of radio-loud objects within the NLS1 population and compared it to the fraction of radio-loud sources within the population of broad line Seyfert 1 (BLS1) belonging to the same catalogue, and they found a significant difference (~ 7 per cent of radio-loud AGN, among NLS1, and 20 per cent among BLS1). On a more general basis, the fraction of radio-loud AGN seems to depend both on the mass of the central SMBH (e.g. Chiaberge & Marconi 2011) and on the accretion rate relative to the Eddington limit: large SMBH masses combined to low accretion rates are believed to give the highest probability of producing AGN with large values of radio-loudness while AGN characterized by high accretion rates and small SMBH masses, like NLS1, seem to be less effective in producing radio-loud sources (e.g. Lacy et al. 2001; Sikora, Stawarz & Lasota 2007).

A second characteristic of the few RL NLS1 discovered so far is that most of them present a compact radio emission (linear size below a few kpc, e.g. Doi et al. 2012 and references therein). Among the most radio-loud NLS1 there are many cases showing strict similarities with the class of blazars (BL Lac objects and flat spectrum radio quasar, FSRQ): like blazars, these RL NLS1 show a flat or inverted radio spectrum, high brightness temperatures ($T_b > 10^7$ K, e.g. Doi et al. 2013; Yuan et al. 2008) and they are detected in gamma-rays by *Fermi*-LAT (Abdo et al. 2009a,b; Foschini 2011). Since blazars are usually believed to be radio galaxies whose relativistic jets are pointing towards the observer (e.g. Urry & Padovani 1995), a possible conclusion is that also some of the RL NLS1 discovered so far are “oriented” and relativistically beamed sources. In this case we must expect a large number of mis-oriented and unbeamed sources, the so-called parent population, that in the standard beaming model is constituted by the class of lobe-dominated radio galaxies. To date, however, only in six RL NLS1 an extended emission has been detected (Whalen et al. 2006; Antón, Browne & Marchã 2008; Doi et al. 2012) and only one RL NLS1 (SDSSJ120014.08–004638.7) is a lobe-dominated FR II radio galaxy (Doi et al. 2012). It is not clear whether the lack of RL NLS1 in radio-galaxies is suggesting an intrinsic difference with respect to the other RL AGNs or if it is just a selection effect: if the BLR has a disk-like geometry, as suggested by some authors (e.g. Pozo Nuñez et al. 2013; Decarli et al. 2008), then selecting AGN with the narrowest emission lines may preferentially lead to the selection of face-on systems and, therefore, with blazar-like radio morphology, in case of radio-loud AGNs. Alternatively, RL NLS1 are intrinsically different from more powerful RL AGN and lacking any extended emission. In this case, the mis-oriented population could appear as NLS1 with very weak (since unbeamed) radio cores i.e. sources classified as RQ NLS1 (Foschini 2013). Another interesting possibility is that RL NLS1 are young or “frustrated” radio-galaxies that have not yet formed (or they are not able to form) radio lobes on large scales. This possibility is suggested by the similarities found between the class of RL NLS1 and that of the compact steep-spectrum (CSS) sources or the gigahertz-peaked spectrum (GPS) sources (e.g. Oshlack, Webster & Whiting 2001; Gallo et al. 2006; Komossa et al. 2006; Yuan et al. 2008).

Clearly, a deeper investigation of the RL NLS1 and, in particular, of the candidates for the parent population is mandatory to discriminate among the various possibilities and to unveil the true nature of this class of AGN. To date, only a few RL NLS1

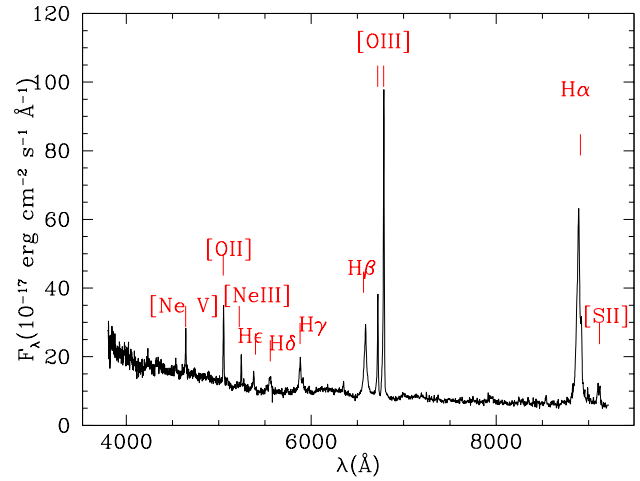


Figure 1. Optical (SDSS) spectrum in the observer’s frame of SDSSJ143244.91+301435.3 ($z=0.355$). The strongest emission lines are labeled.

with non-blazar properties (e.g. with steep radio spectra) have been discovered and studied. This number reduces to just few units if we require a value of the radio loudness parameter that unambiguously sets them in the class of radio-loud AGN (e.g. $R_{1.4\text{GHz}} > 100$, Yuan et al. 2008; Komossa et al. 2006).

In this paper, we present the discovery of a rare example of RL NLS1 (SDSSJ143244.91+301435.3, $z=0.355$) with a radio-loudness parameter well in the radio-loud regime ($R=160$, computed at 5 GHz, and $R_{1.4} \sim 600$, computed at 1.4 GHz) and showing non-blazar properties. The study of this newly discovered object may help in shedding light on the possible nature of the parent population of this peculiar class of AGN. In Section 2 we discuss the optical classification on the basis of the SDSS spectrum, while in Section 3 we study the properties of the host galaxy. In Section 4 we estimate the physical properties of the central SMBH, i.e. its mass and the accretion rate normalized to the Eddington limit. In Section 5 we analyse the radio data trying to disentangle the contribution from different sources present in the field while in Section 6 we search for high-energy (gamma-ray and X-ray) emission from SDSSJ143244.91+301435.3 by exploiting the existing public catalogues (ROSAT, *XMM-Newton*, *Fermi*-LAT). Discussion and conclusions are reported in Section 7.

Along the paper we assume a flat Λ CDM cosmology with $H_0=71 \text{ km s}^{-1} \text{ Mpc}^{-1}$, $\Omega_\Lambda=0.7$ and $\Omega_M=0.3$. Errors are given at 68 per cent confidence level.

2 SPECTRAL ANALYSIS

The source SDSSJ143244.91+301435.3 is spectroscopically classified as QSO at $z=0.3548$ in the Sloan Digital Sky Survey (SDSS, DR7). We have analysed the optical spectrum (Fig. 1) to derive a more detailed classification and to obtain some fundamental quantities, like the mass of the SMBH (M_{BH}). In particular, we have analysed the $H\beta$ spectral region which is critical to classify the source as NLS1 and also to derive a reliable SMBH mass using the single-epoch (SE) method (Vestergaard & Peterson 2006).

Historically an AGN is classified as NLS1 when the $H\beta$ emission line is relatively narrow ($\text{FWHM} < 2000 \text{ km s}^{-1}$) compared to typical type 1 AGN. As type 1 AGN, instead, NLS1 have a low $[\text{OIII}]\lambda 5007\text{\AA}/H\beta$ flux ratio (< 3) that distinguishes them

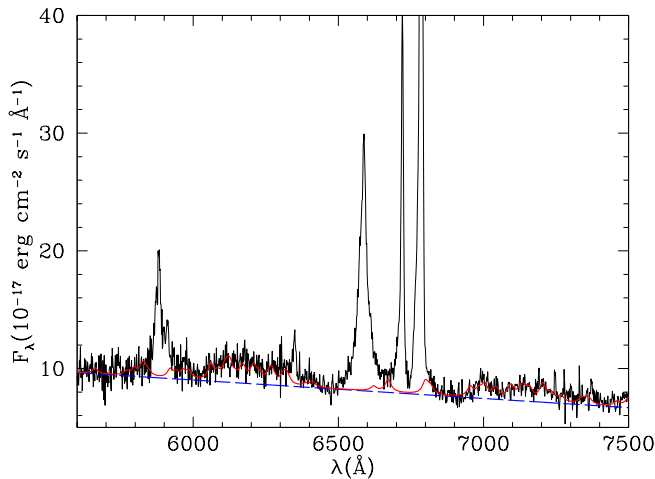


Figure 2. Result of the spectral analysis around the $H\beta$ region aimed at estimating the intensity of the iron emission at 4570\AA . The dashed line (blue in the electronic version) is the fitted continuum while the solid line (red in the electronic version) indicates the continuum+iron emission based on the iron template presented in Véron-Cetty, Joly & Véron (2004).

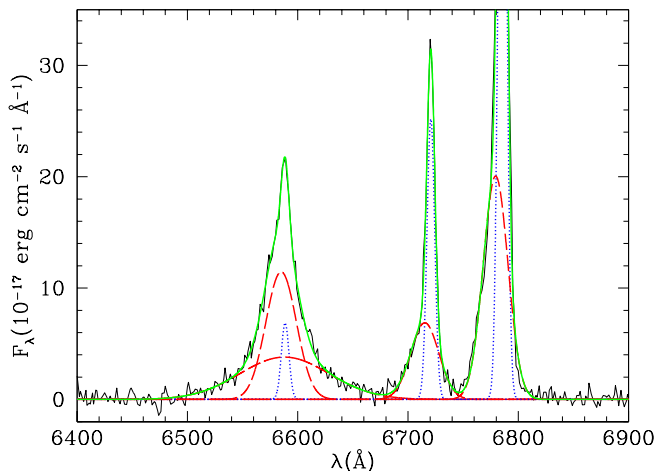


Figure 3. Iron and continuum subtracted spectrum around the $H\beta$ region. The results of the fitting procedure described in the text are also shown. Dotted lines are the narrow components (blue in the electronic version), dashed lines (red in the electronic version) represent the two broad components of $H\beta$ and the broad blue wings of the two [OIII] lines, the solid line (green in the electronic version) represents the total fit.

from absorbed (type 2) AGNs. Usually NLS1 present also strong iron emission although this is not universally accepted as a defining property of the class. The strength of the iron emission at 4570\AA with respect to the $H\beta$ line flux (broad plus narrow component), the so-called R_{4570} parameter, is typically larger than 0.4 (Véron-Cetty, Véron & Gonçalves 2001).

A simple fit with a Lorentian profile of the $H\beta$ yields a FWHM of 1370 km s^{-1} . However the probable presence of a narrow component of $H\beta$ may lead to an underestimate of the actual width of the broad component. An accurate determination of the width of the broad component of $H\beta$ is required also to correctly derive M_{BH} .

In order to characterize the actual width of the broad component of $H\beta$ line and also to estimate the intensity of the iron emission we analyse the spectral region around the $H\beta$ using a

multicomponent method similar to that described in Shen et al. (2011) and Caccianiga et al. (2013): first, we fit the spectrum in the 5600\AA - 7500\AA range, avoiding the regions where the emission lines are present, using a combination of a power-law continuum and an iron pseudo-continuum template presented in Véron-Cetty, Joly & Véron (2004) (see Fig. 2). Then, we subtract this template from the spectrum and fit the result in the observed spectral range between 6400 - 7000\AA using a model composed of several Gaussians: the two [OIII] lines are fitted with 4 Gaussians, two for the cores and two to fit the observed blue wings¹ (e.g. Denney et al. 2009; Shen et al. 2011). The relative intensity of the two Gaussians describing the cores of the [OIII] emission lines is fixed to the theoretical value of 3:1. The narrow component of $H\beta$ is described by one Gaussian whose width is forced to be the same of the narrow [OIII] $\lambda 5007\text{\AA}$ line. For the broad component of $H\beta$ we initially use a single Gaussian which, however, does not reproduce correctly the $H\beta$ profile. The fact that the broad $H\beta$ in AGN is not well represented by a single Gaussian has been often pointed out (e.g. Sulentic, Marziani & Dultzin-Hacyan 2000; Collin et al. 2006) and it is particularly true for AGN belonging to the population A i.e. AGN with a broad component of the $H\beta$ with $\text{FWHM} < 4000\text{ km s}^{-1}$. The profile is usually fitted using a Lorentian function or several Gaussians. We obtain a good fit to the data using two Gaussians. The lines positions are all independent, i.e. we have not fixed the relative distances. We have found that the relative positions of the cores of the narrow lines are all consistent, within 6 - 7 km/s , with the expected values while, as described below, we have found some significant offsets of the broad components with respect to the cores. The result of the fit is presented in Fig. 3.

In this fit the broad $H\beta$ component (which is the sum of two Gaussians) has a FWHM, corrected for the instrumental resolution, of 1776 km s^{-1} , a value typical for the NLS1 galaxies. The measured [OIII] $\lambda 5007\text{\AA}/H\beta$ flux ratio (1.5) is in the range of values observed in unabsorbed AGN (type 1 AGN and NLS1). From the spectral modelling we obtain also a value of the intensity of the iron emission (R_{4570}) equal to ~ 0.45 which is, again, in the typical range observed in NLS1 (Véron-Cetty, Véron & Gonçalves 2001).

The fitting procedure described above has clearly revealed the presence of broad wings on the blue side of both [OIII] narrow lines (see Fig. 3). The wings have a width (FWHM) of 1160 - 1340 km s^{-1} and an offset relative to the line core² of 250 - 270 km s^{-1} . Véron-Cetty, Véron & Gonçalves (2001) found a blue wing in 13 out of 59 NLS1 (22 per cent of the sample) with a range of widths between 525 and 1790 km s^{-1} and offsets ranging from 90 to 570 km s^{-1} . It is believed that these blue wings are originated from bi-conical structures that are outflowing from the nucleus with speeds of a few hundreds of km s^{-1} while the narrow core of the [OIII] lines is expected to follow the kinematics of the stars in the host galaxy (Véron-Cetty, Véron & Gonçalves 2001). In AGN with a relativistic jet the structured shape of the [OIII] lines can also be the result of the interaction of the relativistic jet with the interstellar medium (e.g. Gelderman & Whittle 1994; Holt, Tadhunter & Morganti 2008; Kim et al. 2013).

¹ The presence of blue wings in the [OIII] lines is particularly important in NLS1 (see, e.g., Véron-Cetty, Véron & Gonçalves 2001 and Komossa & Xu 2007)

² We note that, due to the intensity of the AGN emission, we do not observe any absorption line from the host galaxy in the optical spectrum. For this reason we report the observed offsets relative to the cores of the narrow line and not relative to an “absolute” reference frame like the one usually offered by the host galaxy lines

Finally, we have analysed the $H\alpha$ line. Similarly to what was done for the $H\beta$, we have modelled this line with 3 Gaussians, one for the narrow component and two for the broad component. Two additional Gaussians are used to model the [NII] lines at 6583Å and 6548Å, respectively. The relative intensity of these two lines has been fixed to the theoretical value of 2.96. The width of all the narrow lines has been fixed to be equal to the line width of [OIII] (adjusted for the spectral resolution). One of the two Gaussians describing the broad component of $H\alpha$ is found to be offset with respect to the narrow component ($\sim 10\text{\AA}$ corresponding to $\sim 330\text{ km s}^{-1}$), although the significance of this offset is marginal. The FWHM of the broad component of $H\alpha$ is $\sim 1760\text{ km s}^{-1}$ a value very similar to the width of the broad component of the $H\beta$.

We conclude that SDSSJ143244.91+301435.3 can be confidently classified as NLS1 based on the $H\beta$ and $H\alpha$ line widths and on the basis of the [OIII] $\lambda 5007\text{\AA}/H\beta$ flux ratio. Moreover, the source presents other peculiar properties, like the intensity of the iron emission and the presence of blue wings in the [OIII] emission lines, that are typical of this class of AGN.

3 PROPERTIES OF THE HOST GALAXY

One important issue related to the RL NLS1 is about the galaxy type hosting these AGN. On the one hand, RQ NLS1 are usually associated with spiral hosts that often show intense star-forming activity (e.g. Deo, Crenshaw & Kraemer 2006; Sani et al. 2010, 2012) and, on the other hand, radio-loud objects (at least the most radio-loud ones) are usually hosted by early-type galaxies (e.g. Sikora, Stawarz & Lasota 2007 and references therein).

The origin of the dichotomy in the morphology of the host galaxy of RQ and RL AGN is not yet clear but there are indications suggesting that it could be related to the different accretion history of the two classes of galaxies that eventually affects the final value of the spin of the central SMBH: many small mass accretion events in disk galaxies and major mergers in ellipticals (Volonteri, Sikora & Lasota 2007; Sikora 2009). The latter process is expected to produce more easily large values of spin in the central SMBH a condition that is likely connected to a greater efficiency in producing relativistic jets (“spin paradigm”, Blandford 1990).

The peculiar combination of a radio-loud AGN with NLS1 properties opens the question of what kind of galaxy is hosting these objects. So far, only in very few RL NLS1 the host galaxy has been studied and characterized (Zhou et al. 2007; Antón, Browne & Marchã 2008; Hamilton & Foschini 2012; Foschini et al. 2012). These observations have revealed the existence of arms or circumnuclear rings (possibly the consequence of a recent merger) and the presence of a circumnuclear starburst. These results seem to suggest that the galaxies hosting these RL NLS1 are more similar to those typically observed in the radio-quiet counterparts but it is still premature to derive any firm conclusion.

For the reasons explained above, it is interesting to study the properties of the host galaxy of SDSSJ143244.91+301435.3. We do it, both using the SDSS images and by analysing the Spectral Energy Distribution (SED) of the object.

3.1 Radial profile

We have analysed the multi-band SDSS-DR9 images. A 2-D modelling, using the GALFIT package (Peng et al. 2002, 2010), was performed in each band, where different Sersic profiles were tentatively fitted. The results show that the object is best modelled

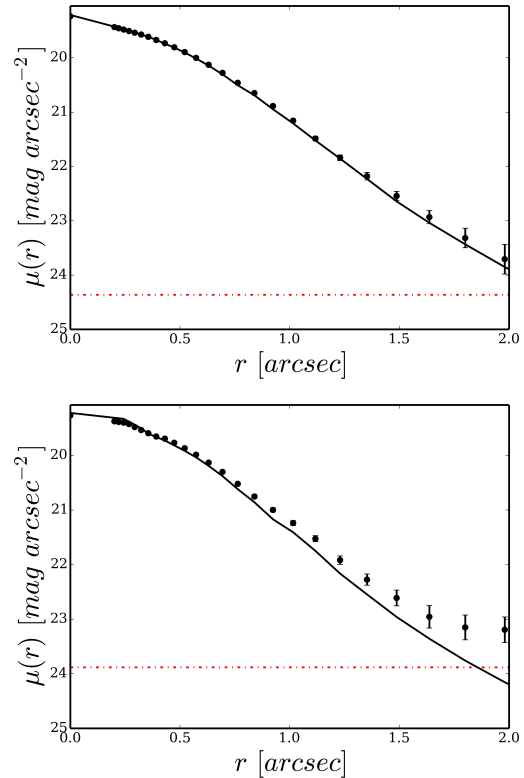


Figure 4. Radial profile in the SDSS r -band (top) and in the i -band (bottom) of SDSSJ143244.91+301435.3. The PSF profile is indicated with the solid line while the red dashed dotted line represents the background.

by a PSF. The latter is reconstructed from the images provided by SDSS, on all five bands. Similar results were found after testing different PSF models, namely by building our PSF from the field image using the IRAF daophot package and by stacking bright, non-saturated and isolated stars of the field. In Fig. 4 we present the 1-D profiles in r and i -band. The surface brightness profiles were derived from the ellipse STSDAS routine and then converted to mag arcsec^{-2} via

$$\mu = -2.5 \text{Log} \left(\frac{I}{s^2 t_{exp}} \right) + m_{zpt} \quad (1)$$

where I is the output profile from ellipse, $s=0.396\text{ arcsec/pixel}$ is the plate scale of the SDSS, t_{exp} is the exposure time and m_{zpt} is the magnitude zero-point all extracted from the image header. The error bars of the profile include two distinct terms. One is the propagated error from the derived flux profile and the second term takes into account the background noise. The model profiles match the observed profiles closely with the exception of the i -band profile where a greater deviation from the PSF profile might be indicative of an excess of emission from the host galaxy (see Fig. 4, lower panel) at the wavelength of 7625Å (corresponding to 5627Å, rest-frame). However, GALFIT cannot converge on any meaningful solution, thus, no structural parameters can be derived.

3.2 Optical and IR SED modelling

The analysis of the optical images of SDSSJ143244.91+301435.3 has not allowed us to derive information about the type of host galaxy but it suggested that in the reddest part of the spectrum the

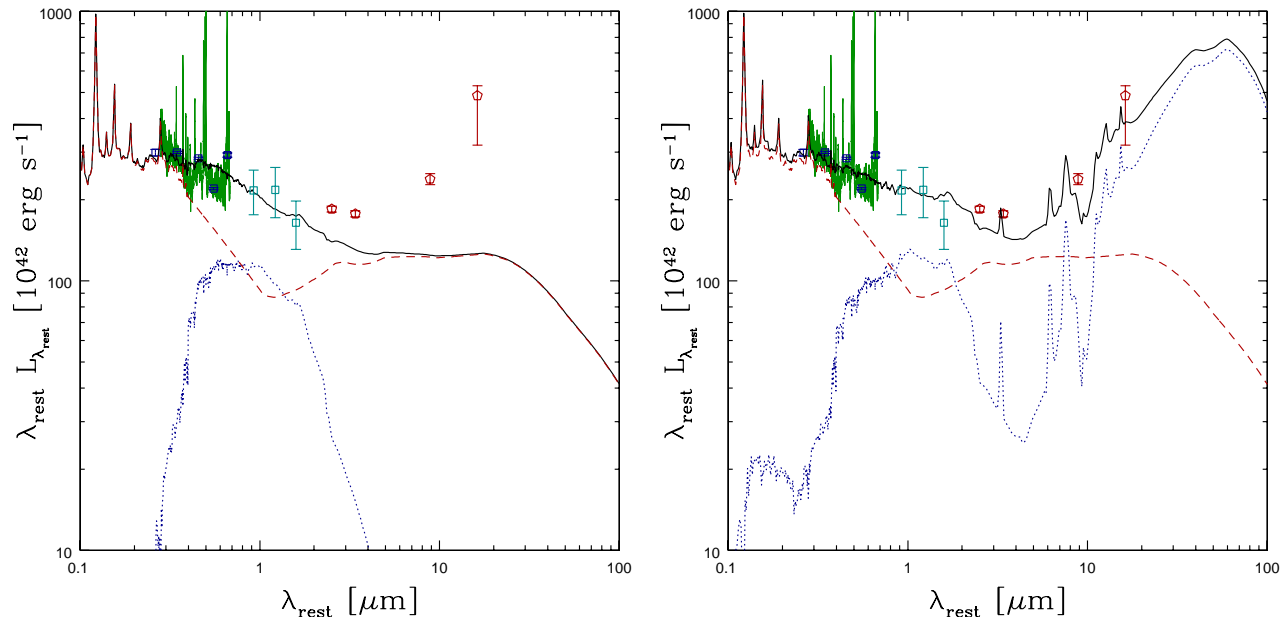


Figure 5. Spectral Energy Distribution of SDSSJ143244.91+301435.3, in the visible/IR range. Photometric points are taken from SDSS (visible; blue points in the colour version), 2MASS (NIR; cyan points in the colour version) and WISE (MIR; red points in the colour version). The optical (SDSS) spectrum is also plotted (green line in the colour version). The solid line is the model that better reproduces the data, and it is composed of an AGN template (BQSO1 from Polletta et al. 2007, dashed red line) plus a galaxy template (dotted blue line): in the left panel an elliptical galaxy template is used while, in the right panel, we adopt a starburst galaxy template (M82). See text for details.

galaxy could be becoming more and more important. This means that a proper analysis of the Spectral Energy Distribution (SED) of SDSSJ143244.91+301435.3, including infrared (IR) photometric data, may reveal some useful hints about the type of host galaxy. We have thus built the SED of SDSSJ143244.91+301435.3 from optical to IR wavelengths using the photometric points from the available catalogues. Besides the *SDSS* photometric data, magnitudes in the *J*, *H*, and *K*, 2MASS bands are available (see Tab. 1). At longer wavelength, IR information are provided by the Wide-field Infrared Survey Explorer (Wright et al. 2010), a NASA satellite that imaged the whole sky in four mid-IR photometric bands, centred at 3.4, 4.6, 12 and 22 μm . We refer to these bands as W1, W2, W3 and W4, respectively. A WISE object, at a distance of 0.17'' from the optical position of SDSSJ143244.91+301435.3, is detected in all four bands with high significance (S/N of 38.9, 37, 24.7, and 12.8 in W1, W2, W3 and W4, respectively). In Tab. 1 we report the profile-fit photometry as obtained from the WISE All-Sky source catalog; the corresponding flux densities have been computed by assuming the magnitude zero points of the Vega system corresponding to a power-law spectrum ($f_\nu \propto \nu^\alpha$) with $\alpha = -1$. The differences in the computed flux densities expected using flux correction factors that correspond to $\alpha = 1, 0$ or -2 (lower than 0.8 per cent, 0.6 per cent, 6 per cent, and 0.7 per cent in W1, W2, W3 and W4, respectively) have been added to the catalogued flux errors. To account for the observed discrepancy between the red and blue calibrators used for the conversion from magnitudes to Jansky, an additional 10 per cent uncertainty was added to the 12 and 22 μm flux densities (Wright et al. 2010).

In order to deconvolve the galaxy and AGN contributions, we adopted a very simple phenomenological approach: The SED has been modelled by the sum of a galaxy and an AGN template chosen from the SWIRE template library of Polletta et al. (2007). We overplotted the model on the SED and chose the combination of

templates that better reproduced the data. The AGN templates have been derived by combining the *SDSS* quasar composite spectrum and rest-frame IR data of a sample of optically-selected type 1 QSOs observed in the SWIRE program. We considered three templates with the same optical spectrum but three different IR SEDs: a mean IR spectrum, obtained from the average fluxes of all measurements (“QSO1”), a template with high IR/optical flux ratio template, obtained from the highest 25 per cent measurements per bin (“TQSO1”), and a low-IR emission SED obtained from the lowest 25 per cent measurements per bin (“BQSO1”). The continuum and the broad line components of the AGN template were absorbed with the extinction curve taken from Chiar & Tielens (2006). The best representation of the AGN continuum is obtained using an A_V of 0.1 mag. For the galaxy emission, we considered 16 templates, covering the wavelength range between 1000 \AA and 1000 μm . They include 3 ellipticals, 7 spirals (from early to late types, S0-Sdm), and 6 starburst templates. When overplotted on the top of the spectrum, the *SDSS* photometric points look fairly consistent (see Fig. 5, left panel), suggesting that the 3'' fiber includes most of the source flux. Therefore, we included also the spectrum in the SED modeling. At short wavelength, the observed fluxes are clearly dominated by the emission from the active nucleus. In order to correctly describe the optical spectrum and the *SDSS* photometric points without overestimating the emission at 3.4, 4.6, and 12 μm , we have to adopt the “BQSO1” template. Starting from the *i* and *z* *SDSS* bands the observed SED requires an additional contribution that becomes particularly important in the 2MASS energy range. This contribution is probably due to the emission from the host galaxy that is more and more important in the red part of the *SDSS* spectrum. This is independently confirmed by the analysis of the radial profile of SDSSJ143244.91+301435.3, discussed in the previous section, where we have found that in the *i*-band there is an indication of the presence of some extended emission (contrary to what is observed

Table 1. IR data.

2MASS				WISE				
Name	<i>J</i>	<i>H</i>	<i>K_s</i>	Name	3.4 μm	4.6 μm	12 μm	22 μm
(1)	(2)	(3)	(4)	(5)	(6)	(7)	(8)	(9)
958046664	17.20±0.21	16.42±0.23	15.88±0.22	J143244.92+301435.3	14.46±0.03	13.54±0.03	10.32±0.04	7.46±0.09

Col. (1): 2MASS All-Sky Release PSC key. Col. (2)-(4): 2MASS magnitudes, not corrected for Galactic extinction. Col. (5): WISE source designation. Col. (6)-(9): WISE magnitudes, not corrected for Galactic extinction.

at shorter wavelengths). While any host template is able to reproduce the photometry observed up to $\sim 4 \mu\text{m}$ (rest frame), the W3 and particularly the W4 data clearly require a galaxy with a significant star-formation (SF) emission. The best representation of the data (see Fig. 5, right panel) is obtained using the template of M82.

It is interesting to estimate the star-formation rate (SFR) from the intensity of the IR emission of the host galaxy. From Kennicutt (1998) we can infer the SFR from the integrated 8-1000 μm luminosity (L_{FIR}):

$$\frac{SFR}{M_{\odot}y^{-1}} = 4.5 \times 10^{-44} \frac{L_{FIR}}{ergs^{-1}} \quad (2)$$

By integrating the M82 template, normalized as in Fig. 5, we obtain a $L_{FIR}=1.13 \times 10^{45} \text{ erg s}^{-1}$ that implies a SFR of $\sim 50.8 M_{\odot} y^{-1}$. Given the value of L_{FIR} inferred from the SED, SDSSJ143244.91+301435.3 can be classified as Luminous Infrared Galaxy (LIRG, e.g. Sanders & Mirabel 1996).

The presence of a star-forming host galaxy is in agreement with what is usually found in RQ NLS1. In particular, Sani et al. (2010) has found that SF is usually higher in NLS1 galaxies than in BLS1 galaxies with the same nuclear luminosity. Using our SED modelling we have estimated the SF vs AGN luminosity ratio as measured by the parameter (Sani et al. 2010):

$$R_6 = \frac{L(6.2, PAH)}{\nu L_{\nu}(6, AGN)} \quad (3)$$

where $L(6.2, PAH)$ is the luminosity of the polycyclic aromatic hydrocarbon (PAH) line at $6.2 \mu\text{m}$ and $\nu L_{\nu}(6, AGN)$ is the AGN luminosity at $6 \mu\text{m}$. We obtain $R_6=0.02$ which is in the typical range of values observed in NLS1 galaxies and close to the median value measured for this class of AGN. On the contrary, BLS1 usually present values of R_6 below 0.01 (e.g. see Fig. 3 in Sani et al. 2010). We note that the value of R_6 reported here is just an estimate based on the SED modelling and it is not computed from an IR spectrum. In particular, the equivalent widths of the lines in the real spectrum could be different from those in the adopted template. However, the good agreement between the estimated R_6 and the value expected in NLS1 can be considered as a support of the reliability of our SED modelling.

3.3 Independent estimate of the extinction

The SED modelling described in the previous section has revealed a low value of optical extinction ($A_V \sim 0.1 \text{ mag}$) in the AGN component. This value is relatively well constrained since, with A_V greater than $\sim 0.3 \text{ mag}$, we cannot reproduce the SED in an acceptable way. At the same time, the SED modelling requires the presence of a high level of SF (that is usually associated to high values of extinction). The two results are not in contradiction since SF in the host of NLS1 is often observed in extended structures, like bars (e.g. Deo, Crenshaw & Kraemer 2006), that do not necessarily intercept the line of sight between the observer and the active

nucleus. Therefore, the AGN could be relatively free from reddening even if the host galaxy is undergoing an intense SF. In order to have an independent confirmation that the nuclear extinction is actually low, we have used the spectral analysis presented in Section 2 to estimate the A_V from the Balmer decrement i.e. the ratio between $H\alpha$ and $H\beta$ fluxes. Since the narrow emission lines are expected to be contaminated by the SF emission³, we have used the broad emission lines. It should be noted, however, that the determination of the amount of reddening using the broad emission lines is difficult because of the high uncertainty on the theoretical value of the intrinsic $H\alpha/H\beta$ flux ratio in the BLR. While this value is quite well determined for the NLR of AGN ($F(H\alpha)/F(H\beta)=3.1$, e.g. Gaskell & Ferland 1984), in the BLR it is expected a value larger than 3.1, as discussed in Maiolino et al. (2001). Therefore, the A_V computed from the broad emission lines, assuming an intrinsic $F(H\alpha)/F(H\beta)=3.1$, should be considered only as an upper limit to the actual value. Using the broad components of the $H\alpha$ and $H\beta$ lines as derived from the spectral analysis presented in Section 2 and corrected for the Galactic reddening, we have computed a Balmer decrement of 2.7 ± 1 . Considering the maximum value of this ratio at 1σ (3.7), and assuming an intrinsic decrement of 3.1 we obtain an upper limit on the A_V of $\sim 0.5 \text{ mag}$. We thus confirm that the nuclear extinction is relatively low and consistent with what has been found in the SED modelling.

As mentioned above, we expect that the SF contributes significantly to the observed narrow emission lines. Therefore, the Balmer decrement computed using the narrow lines could give indications of the extinction in the regions where the SF occurs. The observed Balmer decrement using the narrow components (corrected for the Galactic reddening) is 4.1 ± 1.8 . The large uncertainty on this value is due to the difficulty of measuring the narrow components of the lines, in particular of the $H\alpha$. Using this Balmer decrement we estimate $A_V \sim 0.9 \text{ mag}$ (with a 1σ uncertainty interval of 0 – 2 mag). A value of $A_V \sim 0.9 \text{ mag}$ is consistent with what is usually observed in starburst galaxies (e.g. Kennicutt 1998; Buat et al. 2002; Domínguez et al. 2013; Ibar et al. 2013) and this confirms that a significant fraction of the observed narrow $H\alpha$ and $H\beta$ is probably produced in the star-forming regions of the host galaxy.

4 PROPERTIES OF THE SMBH

From the $H\beta$ width we can compute the mass of the SMBH using the single-epoch relation presented in Vestergaard & Peterson (2006):

³ Using the relation between SFR and $H\alpha$ luminosity in star-forming galaxies (Kennicutt 1998) we have estimated that more than 80 per cent of the narrow component of the $H\alpha$ could be produced by the SF (assuming $SFR=50 M_{\odot} y^{-1}$)

$$\text{Log}\left(\frac{M_{BH}}{M_{\odot}}\right) = 6.91 + 2\text{Log}\left(\frac{FWHM(H\beta)}{1000\text{km s}^{-1}}\right) + 0.50\text{Log}\left(\frac{\lambda L_{5100\text{\AA}}}{10^{44}\text{erg s}^{-1}}\right) \quad (4)$$

using the observed $L_{5100\text{\AA}}$ (2.17×10^{44} erg s $^{-1}$) and the FWHM of the broad component of H β (1776 km s $^{-1}$) we find $M_{BH} = 3.8 \times 10^7 M_{\odot}$. The statistical (1σ) uncertainty on the mass, as propagated from the errors on the two input variables (the line width and the 5100\AA luminosity) is 10%. We note, however, that besides the statistical error there is an additional source of uncertainty related to the single-epoch method and that is mainly connected to the unknown geometry and orientation of the BLR (see discussion in Vestergaard & Peterson 2006). This uncertainty, estimated to be about 0.35-0.46 dex, i.e. a factor 2-3 (Park et al. 2012), is much larger than the statistical uncertainty and it should be considered as a more reliable estimate of the actual error on the computed mass.

The observed luminosity at 5100\AA (rest-frame) is likely contaminated by the host galaxy and, therefore, the actual SMBH mass is expected to be lower. At the same time, a correction for the extinction would increase the value of mass. Using the results from the SED modelling described in Section 3, we expect a contribution of the host galaxy to the luminosity at 5100\AA of ~ 33 per cent and an extinction of $A_V \sim 0.1$ mag. If we correct the observed $L_{5100\text{\AA}}$ for both effects we obtain $L_{5100\text{\AA}} = 1.60 \times 10^{44}$ erg s $^{-1}$ corresponding to a corrected SMBH mass of $\sim 3.2 \times 10^7 M_{\odot}$.

The value of M_{BH} reported by Shen et al. (2011) for SDSSJ143244.91+301435.3 is 3.8×10^7 . This value is not corrected for the host galaxy contamination (nor for the extinction, apart from the Galactic one) but an empirical formula is provided (their eq. 1) to estimate the strength of this contamination at 5100\AA . If we use this formula to correct the M_{BH} reported by Shen et al. (2011) we obtain $M_{BH} = 3.2 \times 10^7 M_{\odot}$ which is in very good agreement with our estimate. The value of SMBH mass derived for SDSSJ143244.91+301435.3 is in the typical range of masses observed in the RL NLS1 (Komossa et al. 2006; Doi et al. 2012; Foschini 2012).

Using the bolometric correction ($BC_{5100} = 10.33$) given by Richards et al. (2006) to compute the bolometric luminosity starting from the luminosity at 5100\AA (corrected for the host galaxy contamination) we obtain $L_{bol} = 1.65 \times 10^{45}$ erg s $^{-1}$ and an Eddington ratio of 0.40. In the estimate of the bolometric correction Richards et al. (2006) consider the integrated emission of the AGN composite spectrum from $100 \mu\text{m}$ to 10keV thus including the infrared part of the SED. In the standard view of an AGN the IR emission is usually attributed to the reprocessed emission of the accretion disk and, therefore, it is often excluded from the estimate of the real energetic output of the source. Since the IR hump usually represents about 1/3 of the total emission (Marconi et al. 2004), a more reliable estimate of the actual bolometric luminosity of SDSSJ143244.91+301435.3 is $\sim 1.1 \times 10^{45}$ erg s $^{-1}$ corresponding to an Eddington ratio of ~ 0.27 . The high accretion rate, close to the Eddington limit, observed in SDSSJ143244.91+301435.3 is, again, typical of the NLS1 class.

As previously mentioned, the SMBH mass derived from the virial method, like the single epoch relation mentioned above, can be significantly underestimated in NLS1 if the BLR is disk-like (e.g. Decarli et al. 2008) or if the radiation pressure (important at high Eddington ratios) affects the kinematics of the BLR (Marconi et al. 2008). We use the relation presented in Chiaberge & Marconi (2011) to estimate the SMBH mass once the radiation pressure is taken into account. We find a factor ~ 2 (0.3 dex) larger value of mass ($M_{BH}^{rad} = 6.6 \times 10^7 M_{\odot}$) and a consequently lower Eddington ratio (0.13). The actual importance of the radi-

ation pressure, however, is still matter of debate (e.g. see Netzer 2009).

Independent estimates of the SMBH mass can be derived using the link between the SMBH mass and the stellar velocity dispersion (Gültekin et al. 2009):

$$\text{Log}\left(\frac{M_{BH}}{M_{\odot}}\right) = 8.12 + \text{Log}\left(\frac{\sigma}{200\text{km s}^{-1}}\right)^{4.24} \quad (5)$$

A rough estimate of σ can be inferred from the width of the narrow lines, like the [OIII] $\lambda 5007\text{\AA}$, assuming that the NLR is influenced by the potential of the galaxy and that the gas follows the same kinematics as stars. Using a sample of type 2 AGN selected from the SDSS, Greene & Ho (2005) have shown that, indeed, narrow lines like the [OIII] $\lambda 5007\text{\AA}$ can be used as a proxy for the dispersion velocity of the bulge provided that the blue wings are correctly modelled and removed. Komossa & Xu (2007) and Komossa et al. (2008) have noted that the [OIII] $\lambda 5007\text{\AA}$ width can be used as a proxy for the stellar velocity only in those NLS1 that do not show large blue-shifts⁴ (hundreds of km s $^{-1}$, e.g. Marziani et al. 2003) in the ‘‘core’’ of the [OIII] line (i.e. excluding the wings). These blue-shifts suggest that this line is unsuitable for tracing the stellar velocity in the bulge. In the case of SDSSJ143244.91+301435.3 we observe blue wings, as described in the previous section, but the core of the line does not show any significant offset (< 50 km s $^{-1}$) with respect to the [SII] $\lambda 6716, 6731\text{\AA}$ emission lines. Therefore, the [OIII] $\lambda 5007\text{\AA}$ width can be considered as a reasonably good proxy of the stellar velocity. The [OIII] $\lambda 5007\text{\AA}$ width (excluding the blue wings), corrected for the instrumental resolution, is $\sigma = FWHM/2.355 = 145$ km s $^{-1}$ which leads to a SMBH mass of $3.4 \times 10^7 M_{\odot}$, with a statistical error of ~ 6 per cent but with a much larger uncertainty due to the intrinsic scatter on the M - σ relation (0.44 dex, Gültekin et al. 2009). This value of mass is very close to the one obtained directly from the virial method without taking into account the radiation pressure. Given the large errors involved in all the methods used to derive the SMBH mass it is not possible to test and quantify the importance of the radiation pressure using only one source but we consider the results presented above as an indication that the possible systematics related to the orientation of the source or to the radiation pressure are well within the expected uncertainty related to the SE virial method.

In conclusion, our best estimate of the mass of the central SMBH of SDSSJ143244.91+301435.3 is $3.2 \times 10^7 M_{\odot}$ with an uncertainty (associated to the SE virial method) of ~ 0.4 dex.

5 RADIO EMISSION

5.1 Radio loudness parameter

SDSSJ143244.91+301435.3 is detected in many of the existing radio surveys (see Tab. 3): the NVSS (Condon et al. 1998) and FIRST (Becker, White & Helfand 1995), at 1.4 GHz, the WENSS survey (Rengelink et al. 1997) at 325 MHz and the 7C (Hales et al. 2007) at 151 MHz. The source is not present in the VLA Low-Frequency Sky Survey Redux (VLSSr) catalogue at 74 MHz (Lane et al. 2012) and we have estimated an upper limit of ~ 600 mJy. The source is not detected at higher frequencies (5 GHz) in the GB6 catalogue

⁴ These offsets are computed relative to the [SII] $\lambda 6716, 6731\text{\AA}$ emission lines

Table 2. Radio data-log of the Effelsberg observations

Date	Freq.	Bandwidth	Beam size	Flux density
	(GHz)	(MHz)	(arcsec)	(mJy)
22.07.2013	4.85	500	145	18.3±2.0
	8.35	1100	89	8.0±1.0
	10.45	300	68	5.4±1.0
30.09.2013	2.64	80	276	38.0±2.0
	10.45	300	68	7.3±1.2

(Gregory et al. 1996). In order to have information also at these frequencies we have observed SDSSJ143244.91+301435.3 with the Effelsberg 100-m radio telescope at 2.64, 4.85, 8.35 and 10.45 GHz (see the observing log in Tab. 2). The source has been detected at all frequencies.

A rough indicator of the level of radio-loudness of the source is the radio-loudness parameter defined as in Kellermann et al. (1989):

$$R = \frac{S_{5\text{ GHz}}}{S_{4400\text{ \AA}}} \quad (6)$$

where the $S_{5\text{ GHz}}$ is the observed flux density at 5 GHz and $S_{4400\text{ \AA}}$ is derived from the B magnitude ($S_{4400\text{ \AA}} = 4.53 \times 10^{-0.4B+6}$ mJy, according to Kellermann et al. 1989). Using the SDSS g and u magnitudes to estimate the B magnitude (Jester et al. 2005):

$$B = g + 0.17 \times (u - g) + 0.11 \quad (7)$$

we obtain $R \sim 160$ a value well above the radio-loud/radio-quiet dividing line ($R=10$) proposed by Kellermann et al. (1989).

This value of R is useful for a comparison with previous works but it is just a crude approximation of the actual radio-to-optical flux density ratio of the source since it is based on observed flux densities, i.e. not k -corrected. To have a more accurate number and for an easier comparison with recent samples of RL NLS1, we have estimated the value of $R_{1.4}$ at 1.4 GHz according to Yuan et al. (2008):

$$R_{1.4} = \frac{S_{1.4\text{ GHz}}}{S_{4400\text{ \AA}}} \quad (8)$$

where the flux densities are referred to the source rest-frame. Using the k -corrected⁵ radio and optical flux densities we obtain $R_{1.4} = 560$. Being $R_{1.4}$ defined at lower radio frequency than R its value is usually larger than R .

We note that the flux density at 4400Å could be in part contaminated by the host galaxy and, at the same time, it can be affected by the extinction. The two effects act in the opposite direction, i.e. the presence of the host galaxy increases the observed flux density while the extinction reduces its value. Similarly to what we have done in the estimate of the mass of the SMBH, we can use the results of the SED modelling described in Section 3 to evaluate the two effects. Applying all the corrections and considering the uncertainties on these estimates we obtain $R_{1.4\text{ GHz}} \sim 600 \pm 100$.

The value of $R_{1.4}$ clearly puts this source among the most

radio-loud NLS1 discovered so far. To date, only 13 RL NLS1 with $R_{1.4} \geq 500$ have been discovered (Yuan et al. 2008; Foschini 2011).

5.2 Radio morphology and possible components

The integrated flux density at 1.4 GHz is 50.6 mJy, in the NVSS, and 50.0 mJy, in the FIRST. The source is barely resolved in the FIRST survey which has a higher angular resolution than NVSS. In the FIRST catalogue the source has a de-convolved size of 0.28'' (major axis) that should be considered as an upper limit of the source size. This limit corresponds to a linear size of 1.4 kpc.

At low-frequency (325 MHz), the source is detected with a peak flux density of 166 mJy/beam and an integrated flux density of 195 mJy. The discrepancy between the two flux densities (of ~ 17 per cent) may indicate a partial extension at this frequency.

In addition to the radio emission centred on SDSSJ143244.91+301435.3, the NVSS map shows many other radio sources/components in the relatively nearby sky region ($\sim 10'$) as shown in Fig. 6. Apart from the radio source associated to SDSSJ143244.91+301435.3 (component 2) some of these additional radio sources are clearly associated to optical objects (components 1 and 4) while other emissions (3 and 5) do not seem to be obviously related to an optical counterpart. In particular, the emission labeled as “3” is quite strong (~ 18.9 mJy of integrated flux density) and relatively close ($\sim 2'$) to SDSSJ143244.91+301435.3. Contrary to the radio source co-incident with SDSSJ143244.91+301435.3, source 3 is clearly extended even at the NVSS resolution (beam size of $\sim 45''$) and it is not detected in the FIRST survey. A possible hypothesis is that source 3 is a radio-lobe associated to SDSSJ143244.91+301435.3 (object A⁶, in the figure). The linear distance between the core and the radio lobe (measured from the peak emission) would be ~ 580 kpc and the source would appear very asymmetric with just one-sided radio lobe.

A second (more likely) possibility, however, is that source 3 is associated to the optical object labeled as B (an early type galaxy at $z=0.2075$) even if not positionally coincident. This is suggested by the fact that source 3 is elongated towards object B. In the FIRST survey this “elongation” is detected as a faint source (component 3b in Tab. 3, $S_{1.4\text{ GHz}} \sim 2$ mJy) positionally coincident with object B (see Fig. 6). It is therefore possible that source 3 is a radio lobe produced by galaxy B rather than SDSSJ143244.91+301435.3. In this case, source 5, another radio source not obviously associated to an optical counterpart, could be the second radio lobe on the opposite side. Under this hypothesis, the linear distance between core and lobe (source 3) is ~ 230 kpc while the total size of the system (i.e. the distance between the two lobes) is ~ 720 kpc. All these parameters are perfectly reasonable for a radiogalaxy. Also the optical spectral type of object B, an early type galaxy, is consistent with what is observed in many radiogalaxies.

At this stage it is difficult to establish on a firm ground which of the two hypotheses described above is correct. More radio data are required to detect, for instance, any possible “bridge” between the radio lobe candidate and one of the two possible radio cores. However, we consider as more probable the hypothesis that the radio component 3 is not associated to SDSSJ143244.91+301435.3 since, otherwise, the system would be extremely asymmetric with just one bright lobe on one side. For this reason in the following

⁵ For the radio we use a spectral index of $\alpha=0.93$ (see next section) while for the optical flux density we use the optical spectrum to derive the 4400Å flux density (rest frame)

⁶ We use numbers to indicate the radio components and letters to indicate the optical sources

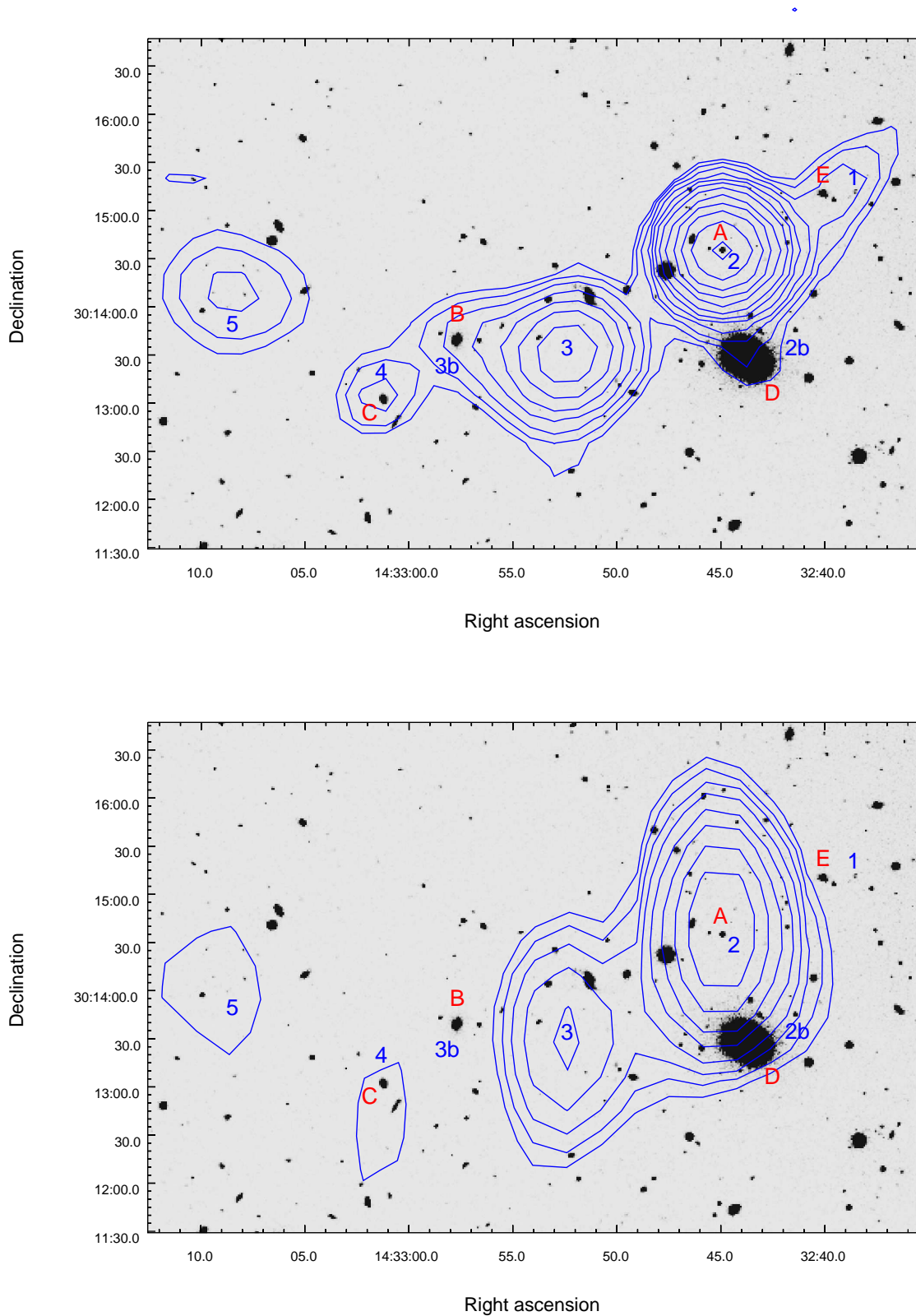


Figure 6. SDSS image in the r-filter with, superimposed, the radio contour levels from NVSS (1.4 GHz, upper panel) and WENSS (325 MHz, lower panel). Contour levels start from 1 mJy (NVSS) and 10 mJy (WENSS) and increase by multiplicative steps of $\sqrt{2}$. The numbers indicate the radio components detected at 1.4 GHz by NVSS (labels 2b and 3b indicate additional components found by FIRST) while letters indicate the optical counterpart candidates. The NLS1 is object A (which is positionally coincident with the radio source 2). North is up, east to the left

Table 3. Radio sources in the field of SDSSJ143244.91+301435.3. Numbers indicate the radio components detected in the NVSS catalogue while a letter after the number indicates a sub-component detected at higher resolution in the FIRST catalogue.

Comp.	$S_{10.45\text{GHz}}$ (Eff.) mJy	$S_{8.35\text{GHz}}$ (Eff.) mJy	$S_{4.85\text{GHz}}$ (Eff.) mJy	$S_{2.64\text{GHz}}$ (Eff.) mJy	$S_{1.4\text{GHz}}^{\text{peak}}$ (NVSS) mJy/beam	$S_{1.4\text{GHz}}^{\text{int}}$ (NVSS) mJy	$S_{1.4\text{GHz}}^{\text{peak}}$ (FIRST) mJy/beam	$S_{1.4\text{GHz}}^{\text{int}}$ (FIRST) mJy	$S_{325\text{MHz}}^{\text{peak}}$ (WENSS) mJy/beam	$S_{325\text{MHz}}^{\text{int}}$ (WENSS) mJy	$S_{151\text{MHz}}$ (7C) mJy
1	-	-	-	-	2.3	5.9	1.27	1.74	-	-	-
2	6.4 ¹	8.0	18.3 (11.7) ²	38.0 (27.6) ²	50.6	50.6	49.94	49.98	166	195	330
2b	-	-	-	-	-	-	0.68	1.04	-	-	-
3	-	-	-	-	10.6	18.9	-	-	45	51	-
3b	-	-	-	-	-	-	2.0	1.4	-	-	-
4	-	-	-	-	2.7	2.7	2.49	2.79	-	-	-
5	-	-	-	-	3.5	3.5	-	-	-	-	-

¹ this is the average value of the two flux densities measured in July and September (see data-log in Table 2).

² the numbers between parenthesis are the flux densities corrected for confusion (contamination from source 3)

discussion we will assume that only the radio emission labeled as 2 is associated to SDSSJ143244.91+301435.3 (this association is certain).

5.3 Radio spectrum

All radio flux densities available/measured for SDSSJ143244.91+301435.3 are reported in Tab. 3 (source 2) and plotted in Fig 7. A least square fit to the data results in a quite steep ($\alpha \sim 0.9$) spectrum. Since, as discussed above, this region of sky is quite crowded (see Fig. 6) it is possible that some of the measured flux densities, in particular those taken with a “single dish” (Effelsberg), are confused by nearby sources. Among all sources which are close enough to SDSSJ143244.91+301435.3 to be potentially contaminating the observed fluxes, two are quite faint (sources 1 and 2b in Tab. 3). Their possible contamination of the flux density of SDSSJ143244.91+301435.3 is expected to be below ~ 10 per cent. The principal contamination is expected to come from source 3 which is relatively strong (18.9 mJy). Given its distance from SDSSJ143244.91+301435.3 ($\sim 2'$) any flux density measured with a beam size $\geq 2'$ is contaminated. The confusion problem, therefore, is likely present in the Effelsberg measurements at the two lowest frequencies (4.85 GHz and 2.64 GHz) where the beam size is 2.4' and 4.6' respectively, while the flux densities at 8.35 and 10.45 GHz should be relatively free from contamination (beam size of 1.5' and 1.1' respectively). We have estimated the contribution of source 3 to the flux density of SDSSJ143244.91+301435.3 (at 4.85 GHz and 2.64 GHz) using the observed NVSS integrated flux density of source 3 at 1.4 GHz (~ 17 mJy, excluding the contribution from source 3b) and extrapolating it to the 2 frequencies using the observed spectral index of this source (see Fig 7). The corrected flux densities are more aligned with the points at lower and higher frequencies, confirming that the contamination from source 3 is actually present at 4.85 GHz and 2.64 GHz at the level estimated from the NVSS data. The fit to the data corrected for the contamination does not change significantly leading to a value of the slope close to the previously measured one ($\alpha=0.93$).

Most of the radio data used in the analysis were taken at different epochs. In principle, variability may play a role and influence the computed spectral index. However, we have several indications that variability in SDSSJ143244.91+301435.3 is not impor-

tant: FIRST and NVSS data (taken in April 1993 and April 1995, respectively) are fully consistent (see Tab. 3) and the 10.45 GHz flux densities taken at Effelsberg in two different sessions (July and September 2012) are consistent with a constant flux density within $\sim 1 \sigma$ (see Tab. 2). Moreover, we have fitted Effelsberg data taken at the same epoch obtaining very similar slopes (0.93 and 0.97). We conclude that current data do not suggest the presence of radio variability in SDSSJ143244.91+301435.3.

Although a simple power-law offers a reasonable description of the spectrum, the measurements at the lowest frequencies seem to suggest a possible flattening of the slope. If we fit only the flux densities at the highest frequencies (> 1 GHz) and extrapolate the fit to lower frequencies, hints for a possible break at ~ 300 MHz seem to emerge (Fig. 7). Using a broken power-law model we obtain a good fit with a break frequency at ~ 300 MHz (corresponding to 400 MHz, rest frame). The spectral indices above and below the break are 1.2 and 0.5, respectively. On the basis of the available data, however, the presence of a turnover at low-frequencies is not statistically significant and it should be considered just as a possible indication.

5.4 SDSSJ143244.91+301435.3 as CSS source

Most of the RL NLS1 discovered so far with radio-loudness parameters similar to the one computed in SDSSJ143244.91+301435.3 present flatter ($\alpha < 0.5$) radio spectra and show indications for the presence of relativistic beaming, something that suggests the presence of a relativistic jet pointing towards the observer (Yuan et al. 2008). For comparison, in the Yuan et al. (2008) sample of very radio-loud NLS1 only one source (J1443+4725), among those with a measured spectral index, has a relatively steep ($\alpha=0.67$) radio spectrum. In the Komossa et al. (2006) sample there are 2 sources (SDSS J172206+565451 and RX J0134-4258) with a high value of radio-loudness and having a steep (0.69-1.4) radio spectrum⁷. The steep radio spectrum observed in SDSSJ143244.91+301435.3 seem to exclude that we are observing

⁷ The source TEX 1111+329 in the Komossa et al. (2006) sample has a very steep spectrum (1.24 between 1.4 and 5 GHz) but the radio-loudness parameter, once corrected for the high level of reddening measured in this object, is ~ 20 i.e. much lower than the one observed in SDSSJ143244.91+301435.3

Table 4. Properties of the possible optical counterparts

name	position (J2000)	u (SDSS)	g (SDSS)	r (SDSS)	i (SDSS)	z (SDSS)	redshift	comments
A	14 32 44.91 +30 14 35.4	19.14	18.82	18.56	18.62	18.11	0.355	NLS1
B	14 32 57.68 +30 13 39.5	20.31	18.83	17.53	16.96	16.59	0.2075	Early type galaxy
C	14 33 01.22 +30 13 02.4	19.45	18.53	18.04	17.66	17.55	-	-
D	14 32 43.90 +30 13 29.2	17.34	15.40	14.52	14.10	13.79	0.0623	Early type galaxy
E	14 32 40.14 +30 15 10.5	21.19	19.69	19.14	18.85	18.75	-	-

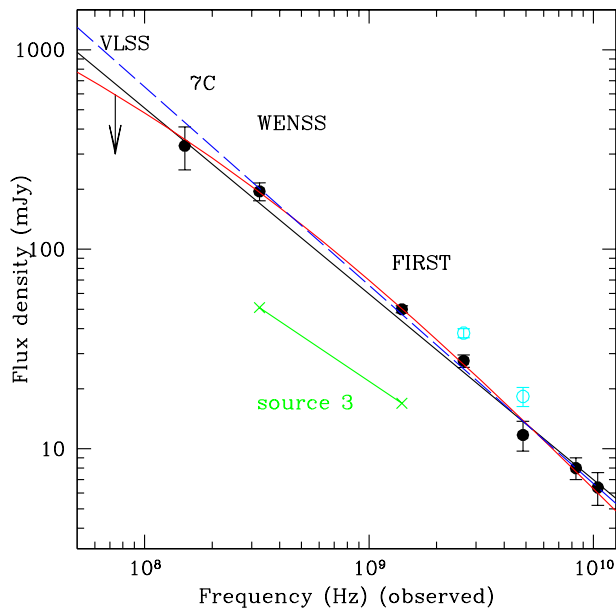


Figure 7. Radio spectrum of SDSSJ143244.91+301435.3. High-frequency data (>2.6 GHz) come from Effelsberg observations while lower-frequency data come from existing catalogues (see labels). The 2 open points (cyan in the electronic version) are the Effelsberg flux densities at 2.64 and 4.85 GHz (where the beam size is larger than $2'$) not corrected for the contamination of the nearby source 3 (whose spectrum is also plotted with the two green crosses and line). The two fits to the points using a single power-law and a smooth broken power-law (with a break at 300 MHz) respectively are also plotted as solid lines (black and red, respectively, in the electronic version). Finally, the dashed (blue) line is the fit to the points at the highest frequencies (>1 GHz).

a jet pointing in our direction. This is further supported by the non-detection of a strong flux variability, as explained earlier. Therefore, SDSSJ143244.91+301435.3 is one of the very few RL NLS1 with a high radio-loudness parameter that could belong to the parent population.

With the observed radio properties the source can be classified as a CSS radio sources (O’Dea 1998; Dallacasa et al. 1995). The radio power of SDSSJ143244.91+301435.3 (2.1×10^{25} W Hz $^{-1}$ at 1.4 GHz) is in the range usually observed in CSS sources (e.g. O’Dea 1998; Fanti et al. 2001). CSS sources have a linear size between 1 and 20 kpc and present a spectral turnover at low (<500 MHz) frequencies attributed to synchrotron self-absorption or free-free absorption. The position of the turnover is inversely correlated with the linear size of the source and, for sources with a linear size of ~ 1.4 kpc, we expect a turnover at ~ 100 -500 MHz (e.g. O’Dea

1998). As previously discussed there is a possible hint (although not statistically significant) of a change of slope at low-frequency (observed at ~ 300 MHz corresponding to 400 MHz, rest frame) that may indicate a possible turnover of the spectrum at a frequency close to the one expected. The observed spectral index (0.93 considering a single power-law fit, or 1.2, considering the broken power-law fit) is within the distribution of indices, measured above the spectral turnover, of the CSS sources (between 0.6 and 1.2, Fanti et al. 1990; O’Dea 1998). Finally, in the NVSS data no significant polarization is found (≤ 1 per cent) something that, again, is consistent with what is observed, at these frequencies, in CSS sources with linear size below ~ 6 kpc (Cotton et al. 2003).

CSS sources are compact systems of sub-galactic sizes that show radio morphologies very similar to those observed in “classical” radio galaxies but on much smaller scales. Interestingly, many CSS sources show distorted morphologies suggestive of interactions with a dense and inhomogeneous environment (Dallacasa et al. 2013; O’Dea 1998). At present, we have no high resolution radio images of SDSSJ143244.91+301435.3 that could confirm, also from the morphological point of view, that SDSSJ143244.91+301435.3 is a true CSS source but, given its steep radio spectrum, it is very likely that the source would appear resolved at VLBI scales.

5.5 Radio emission and SF

In the SED modelling discussed in Section 3 the IR photometric points play an important role to detect and characterize the host galaxy properties. The 12 and $22 \mu\text{m}$ points (corresponding to 8.9 and $16.2 \mu\text{m}$, rest frame), in particular, are critical to establish the possible starburst nature of the host. We have then shown that SDSSJ143244.91+301435.3 presents a strong radio emission that is likely ascribed to the presence of a jet. In principle, the possible presence of a jet could contaminate the observed IR emission leading to incorrect conclusions about the presence of SF in the host galaxy. For this reason, we want to assess the level of this possible contamination in the 1-20 μm spectral region. To this end, we have to assume a radio-to-IR spectral slope. One possibility is to simply extrapolate the slope ($\alpha \sim 0.9$) observed in the radio band up to the IR region. With this slope we predict a flux density at $22 \mu\text{m}$ which is 3 orders of magnitude lower than the one observed. Nevertheless, the radio spectrum is based on the observed emission which is likely dominated by extended components, like mini-lobes, that have steep spectra. The nuclear emission, instead, is expected to have a flatter spectrum, more similar to the one observed in blazars. For this reason, we have also considered the average radio-to-IR slopes derived from the Caltech-Jodrell Bank Flat spectrum (CJ-F, Taylor et al. 1996) sample of blazars. This is a flux limited and complete sample of flat spectrum radio sources with a

radio flux density greater than 350 mJy at 5 GHz. The SED of most of the 293 CJ-F blazars is under study (Antón et al. in prep.). Using the average value of slope between 5 GHz and 22 μm of the CJ-F blazars ($\alpha_{5\text{GHz}}^{22\mu\text{m}}=0.64$) we predict a flux density which is 2 orders of magnitude below the observed value. Even considering the rms uncertainty on the value of this slope we still predict a contribution of jet to the 22 μm flux density which is less than 10 per cent. We conclude that the possible contamination of the jet emission to the observed IR emission is not expected to be significant. The presence of a significant SF is therefore the best explanation for the observed IR emission at $\sim 10\text{-}20\ \mu\text{m}$.

We finally note that a high SF is expected to produce an important radio emission that can represent a relevant contribution to the observed radio luminosity of SDSSJ143244.91+301435.3. If this contribution was significant it could explain the steep radio spectrum observed in SDSSJ143244.91+301435.3. We can estimate the expected radio emission due to the SFR from the following equation (Condon, Cotton & Broderick 2002):

$$\frac{P_{1.4\text{GHz}}}{\text{WHz}^{-1}} \sim 4.6 \times 10^{21} \frac{\text{SFR}(M > 5M_{\odot})}{M_{\odot}\text{y}^{-1}} \quad (9)$$

Using a SFR of $50 M_{\odot} \text{y}^{-1}$ we predict a radio luminosity of $2.3 \times 10^{23} \text{ W Hz}^{-1}$ which is a factor ~ 100 lower than the observed $P_{1.4\text{GHz}}$. A similar value ($1.5 \times 10^{23} \text{ W Hz}^{-1}$) is obtained if we use the radio vs FIR luminosity relation computed for the IRAS Bright Galaxy Sample presented in Condon, Cotton & Broderick (2002). We conclude that the observed radio emission should be only marginally (~ 1 per cent) contaminated by the SF in the host galaxy.

6 HIGH-ENERGY EMISSION

6.1 X-rays

X-rays can provide potentially important pieces of information on SDSSJ143244.91+301435.3. At these energies we expect to observe the nuclear emission typical of RQ AGN, which is likely produced by a hot corona of electrons reprocessing the primary UV-optical emission of the disk via inverse-Compton mechanism (Haardt & Maraschi 1991). In RQ NLS1, in particular, the X-ray emission is often characterized by steeper 2-10 keV slopes, when compared to BLS1 (e.g. Brandt, Mathur & Elvis 1997; Zhou & Zhang 2010; Grupe et al. 2010; Caccianiga et al. 2011), and by the presence of a strong and variable soft-excess at lower energies (< 2 keV, Boller, Brandt & Fink 1996). XMM-Newton observations have also revealed an interesting spectral complexity (spectral drops/curvature) in many NLS1 (e.g. Gallo 2006 and references therein) that has been interpreted as caused either by the presence of dense material in the close environment of the central SMBH (“partial covering model”, e.g. Tanaka et al. 2004) or by the reflection of the primary emission on the accretion disk (“reflection model”, e.g. Fabian et al. 2004).

Besides the coronal emission, we also expect a contribution from the relativistic jet, similar to that observed in blazars. The relative intensity of the RQ and RL components strongly depends on the level of beaming present in the source. In “beamed” RL NLS1 the emission from the jet could be very important or even dominant (e.g. Gallo et al. 2006) while in a “mis-oriented” source like SDSSJ143244.91+301435.3 the jet emission is probably less relevant. In addition, since SDSSJ143244.91+301435.3 is also a possible CSS source, we can expect X-ray emission from the shocked heated IGM caused by the expanding radio jet (e.g. Siemiginowska

2009). Finally, the presence of a quite intense SF can also contribute to the total budget of the X-ray emission.

We have searched for X-ray data from the existing surveys but no detection was found. We can derive an upper limit on the soft (0.1-2.4 keV) X-ray emission of SDSSJ143244.91+301435.3 from the ROSAT all sky survey (Voges et al. 1999) of $\sim 5 \times 10^{-13} \text{ erg s}^{-1} \text{ cm}^{-2}$ and an upper limit in the 2-12 keV band from the XMM-Newton Slew Survey (XSS, Warwick, Saxton & Read 2012) of $\sim 6 \times 10^{-12} \text{ erg s}^{-1} \text{ cm}^{-2}$ (assuming a photon index of 2). These upper limits correspond to limits on the X-ray luminosity of $\sim 2 \times 10^{44} \text{ erg s}^{-1}$ and $\sim 3 \times 10^{45} \text{ erg s}^{-1}$ in the 0.1-2.4 keV and 2-12 keV energy bands, respectively. In order to evaluate whether these limits are low enough to set some useful constraint on the emission of SDSSJ143244.91+301435.3, we estimated the predicted X-ray luminosities from the two main components expected from this object, i.e. the coronal and the jet emission. For what concerns the first component, we start from the bolometric luminosity, derived in the previous sections, combined to the value of X-ray bolometric correction⁸ typically observed in AGN accreting with an Eddington ratio of 0.27, using the relations between K_{bol} and Eddington ratio recently published in Fanali et al. (2013). For the jet component, we use the observed radio power at 5 GHz and assumed the mean value of the radio-to-X-ray luminosity ratio typically observed in flat-spectrum radio quasars (FSRQ, Donato et al. 2001). The expected values of X-ray luminosity in the 0.1-2.4 keV (2-10 keV) energy band are $\sim 7 \times 10^{43} \text{ erg s}^{-1}$ ($\sim 4 \times 10^{43} \text{ erg s}^{-1}$) and $\sim 1 \times 10^{43} \text{ erg s}^{-1}$ ($\sim 6 \times 10^{42} \text{ erg s}^{-1}$) for the coronal and the jet emission, respectively. The emission predicted from the jet should be considered only as an upper limit since most of the radio power observed at 5 GHz is expected to come from extended structures, as previously discussed, and not from the radio core. Both estimates of the X-ray luminosity are more than a factor ~ 100 below the upper limits derived from the XSS and more than a factor ~ 3 below the RASS limit and, therefore, the null detection of SDSSJ143244.91+301435.3 is not surprising. In addition, it should be considered that NLS1 are variable X-ray sources that are sometimes observed in very low flux states (e.g. Grupe et al. 2012) and this may have contributed to the null detection of SDSSJ143244.91+301435.3 in the existing X-ray surveys. Pointed observations with one of the existing X-ray telescopes should be able to detect SDSSJ143244.91+301435.3 and to provide enough counts to carry out a reliable spectral analysis.

6.2 Gamma-rays

An interesting issue related to RL NLS1 is that they have been often found to be gamma-ray emitters, like the class of blazars and radio-galaxies. After the first detection of a NLS1 (PMN J0948+0022) in the *Fermi*-LAT catalogue (Abdo et al. 2009a; Foschini et al. 2010) more cases have been discovered (Abdo et al. 2009b) and the number of RL NLS1 detected in the *Fermi*-LAT catalogue keeps on increasing (see Foschini 2011, 2013). Contrary to many of the RL NLS1 discovered so far, the radio properties of SDSSJ143244.91+301435.3, in particular its steep radio spectrum and the lack of polarization and significant variability, suggest that most of the observed radio emission should come from extended structures, like mini-lobes, and not from the core. Therefore it is reasonable to expect that any gamma-ray emission in this object should be lower than in blazars or in core-dominated RL NLS1 with

⁸ K_{bol} is defined as the fraction between the bolometric luminosity and the X-ray luminosity in the 2-10 keV band

a similar observed radio luminosity. Indeed, so far, *Fermi*-LAT has preferentially detected blazars or radio-galaxies characterized by large core-dominance values (Abdo et al. 2010) with the only exception of two very nearby radio galaxies (Cen A and M87). Also considering SDSSJ143244.91+301435.3 as a “young” CSS source, its detection by *Fermi*-LAT detection can have important implications, as recently discussed by Migliori et al. (2013).

We have thus analysed the *Fermi*-LAT public data⁹ searching for a detection, or an upper limit, of the gamma-ray emission of SDSSJ143244.91+301435.3. *Fermi*-LAT data between August 4, 2008 and August 4, 2013 (5 years) were retrieved from HEASARC and analyzed using the standard procedures¹⁰. Specifically, we used LAT Science Tools v. 9.27.1, with Instrument Response Function (IRF) P7_V6, and the corresponding background files. We selected a 10° -radius region centred on the source coordinates. SDSSJ143244.91+301435.3 and all the sources included in the 2 LAT Catalog (Nolan et al. 2012) spatially localized within this region were taken into account. The likelihood analysis (Mattox et al. 1996) was applied on the LAT data both as a whole integrated over all 5 years and by considering integration bunches one-month long (60 bins). No detection was found in both cases, and we set an upper limit of $F(>100 \text{ MeV}) \leq 2 \times 10^{-9} \text{ ph cm}^{-2} \text{ s}^{-1}$ over the 5-year integration. This upper limit corresponds to an upper limit of the gamma-ray monochromatic luminosity at 100 MeV of $\nu L_\nu(100\text{MeV}) \leq 2.1 \times 10^{44} \text{ erg s}^{-1}$ which is within the range of gamma-ray luminosities observed in blazars or RL NLS1 with a similar radio power (Foschini 2011). Therefore it is not yet possible to derive any conclusion about the differences/similarities between SDSSJ143244.91+301435.3 and the class of “oriented” sources.

7 DISCUSSION AND CONCLUSIONS

SDSSJ143244.91+301435.3 is one of the few (13 in total discovered so far) radio-loud NLS1 with a radio-loudness parameter ($R_{1.4}$) of the order of 500 or greater. The radio emission, however, is different from that usually observed in RL NLS1 with such a high value of R, since it shows a steep ($\alpha=0.93$) spectrum. Based on the size of the radio emission ($\leq 1.4 \text{ kpc}$) this object is a compact radio source. The steep radio spectrum and the lack of strong variability and polarization, instead, disfavor the hypothesis that the observed compactness is due to the orientation of a relativistic jet towards the observer, as in blazars. This makes SDSSJ143244.91+301435.3 one of the few examples of RL NLS1 with non-blazar properties and sets it as an interesting case to study the parent population of these sources.

SDSSJ143244.91+301435.3 hosts a relatively low-mass SMBH ($3.2 \times 10^7 M_\odot$) accreting at a rate close to the Eddington limit (Eddington ratio of 0.27), in agreement with what is typically found in both RQ and RL NLS1 objects. We have also investigated the host galaxy properties through a modelling of the SED. We have found that the AGN dominates the emission in the visible range and at 2-3 μm while the host galaxy shows up in the 0.6-2 μm spectral range (we also detect a hint of extension in the *i*-band image) and in the MIR ($>10 \mu\text{m}$). The best modelling is obtained using a star-forming galaxy template (M82) with a SFR, estimated from the IR emission, of $\sim 50 M_\odot \text{ y}^{-1}$. The presence and the intensity of the SF is in agreement with what is usually observed in radio-quiet

NLS1 (e.g. Sani et al. 2010). Given the presence of the SF we have evaluated whether this could explain the observed radio emission but we have concluded that the SF is expected to contribute only marginally (~ 1 per cent) to the observed radio fluxes. This result, combined to the large value of the radio-loudness parameter, confirms the presence of a jet in SDSSJ143244.91+301435.3.

The compact morphology and the steep radio spectrum are characteristics remarkably similar to those observed in the CSS radio sources. It is nowadays clear that the large majority of CSS (and GPS) sources are young objects in which the radio emitting plasma is digging its way through the ISM of the parent galaxy. Observations of hot-spot advance speed (e.g. Polatidis & Conway 2003 and references therein) and radiative ages (e.g. Murgia 2003; Murgia et al. 1999) for a few tens of objects show typical ages of the order of $10^3 - 10^5$ years for GPS and CSS objects respectively. The association of some RL NLS1 with CSS sources has been already proposed by other authors (Moran 2000; Oshlack, Webster & Whiting 2001; Gallo et al. 2006; Komossa et al. 2006). Yuan et al. (2008) also stressed the similarities between RL NLS1 and CSS sources and suggest that RL NLS1 with a flat radio spectrum could be CSS sources whose jet is pointing towards the observer. Another interesting characteristic that makes SDSSJ143244.91+301435.3 similar to CSS sources is the presence of strong blue wings in the [OIII] $\lambda\lambda 4959\text{\AA}, 5007\text{\AA}$ doublet, with FWHM of the order of 1150-1350 km s^{-1} and offsets, with respect to the core of the lines, of ~ 250 -270 km s^{-1} . The presence of these blue-shifted and broad wings is very common in compact radio objects, including CSS sources (Gelderman & Whittle 1994; Holt, Tadhunter & Morganti 2008; Kim et al. 2013) and it is usually considered as a signature of the impact of a radio jet on the interstellar medium of the host galaxy; a jet-driven outflow is often invoked as the best explanation for the observed blue-shifted, broad wings of the narrow lines (Holt, Tadhunter & Morganti 2008; Nesvadba et al. 2011; Kim et al. 2013). Therefore, in sources like SDSSJ143244.91+301435.3 we might be witnessing the AGN-induced feedback acting in the early stages of the evolution of a radio source.

The hypothesis of CSS sources as the parent population of RL NLS1 would naturally explain why RL NLS1 have been detected as compact radio systems without significant extended emission (except for very few cases). In this framework, SDSSJ143244.91+301435.3 would be oriented at an intermediate angle between face-on and edge-on systems, the former being the flat-spectrum blazar-like RL NLS1 and the latter appearing as CSS sources with an obscured optical spectrum (i.e. type 2 AGN). In the first case, it is difficult to distinguish the CSS source morphology, being the radio emission dominated by the beaming effects; in the second class of sources it is difficult, if not impossible, to establish the NLS1 nature, due to the presence of obscuration. Due to the particular orientation of the source, instead, a detailed radio follow-up of SDSSJ143244.91+301435.3 at m.a.s. resolution can provide important pieces of information about the intrinsic (i.e. not affected by beaming) radio properties of RL NLS1. A systematic search for sources like SDSSJ143244.91+301435.3, where both NLS1 and CSS characteristics can be observed, and a radio follow-up of all these objects is then mandatory to confirm the possible link between CSS sources and NLS1 on a firm statistical basis.

⁹ <http://fermi.gsfc.nasa.gov/cgi-bin/ssc/LAT/LATDataQuery.cgi>

¹⁰ <http://fermi.gsfc.nasa.gov/ssc/data/analysis/scitools/>

ACKNOWLEDGMENTS

We thank Dr. Roberta Paladini for her kind support on the analysis of WISE data, Dr. Ian Browne for useful discussions and the referee for a careful reading of the manuscript. Part of this work is based on observations carried out at the 100-m telescope of the MPIfR (Max-Planck-Institut für Radioastronomie) at Effelsberg. This publication makes use of data products from the Sloan Digital Sky Survey (SDSS), from the Two Micron All Sky Survey (2mass), from the Wide-field Infrared Survey Explorer (WISE) and from many radio surveys (NVSS, FIRST, WENSS, 7C and VLSS). The SDSS is managed by the Astrophysical Research Consortium for the Participating Institutions. WISE is a joint project of the University of California, Los Angeles, and the Jet Propulsion Laboratory/California Institute of Technology, funded by the National Aeronautics and Space Administration. The 2mass is a joint project of the University of Massachusetts and the Infrared Processing and Analysis Center/California Institute of Technology, funded by the National Aeronautics and Space Administration and the National Science Foundation. The National Radio Astronomy Observatory is a facility of the National Science Foundation operated under cooperative agreement by Associated Universities, Inc. The Westerbork Synthesis Radio Telescope is operated by the Netherlands Institute for Radio Astronomy ASTRON, with support of NWO.

Part of this work was supported by the COST Action MP0905 “Black Holes in a Violent Universe”. The authors acknowledge financial support from the Italian Ministry of Education, Universities and Research (PRIN2010-2011, grant n. 2010NHBSBE) and from ASI (grant n. I/088/06/0). The research leading to these results has received funding from the European Commission Seventh Framework Programme (FP7/2007-2013) under grant agreement n.267251 “Astronomy Fellowships in Italy” (AstroFit). S. Anton acknowledges the support from FCT through project PTDC/FIS/100170/2008 and Ciencia2007

References

- Abdo A. A. et al., 2009a, *ApJ*, 707, 727
 Abdo A. A. et al., 2010, *ApJ*, 720, 912
 Abdo A. A. et al., 2009b, *ApJ*, 707, L142
 Antón S., Browne I. W. A., Marchã M. J., 2008, *A&A*, 490, 583
 Becker R. H., White R. L., Helfand D. J., 1995, *ApJ*, 450, 559
 Blandford R. D., 1990, 20. Saas-Fee Advanced Course of the Swiss Society for Astrophysics and Astronomy: Active galactic nuclei
 Boller T., Brandt W. N., Fink H., 1996, *A&A*
 Boroson T. A., 2002, *ApJ*, 565, 78
 Botte V., Ciroi S., Rafanelli P., Mille F. D., 2004, *ApJ*, 127, 3168
 Brandt W. N., Mathur S., Elvis M., 1997, *MNRAS*, 285
 Buat V., Boselli A., Gavazzi G., Bonfanti C., 2002, *A&A*, 383, 801
 Caccianiga A., Fanali R., Severgnini P., Della Ceca R., Marchese E., Mateos S., 2013, *A&A*, 549, 119
 Caccianiga A., Severgnini P., Della Ceca R., Corral A., Fanali R., Marchese E., 2011, *Proceedings of Science (PoS, Trieste, Italy)*, vol. NLS1, Published online at <http://pos.sissa.it/cgi-bin/reader/conf.cgi?confid=126>, id.66
 Calderone G., Ghisellini G., Colpi M., Dotti M., 2013, *MNRAS*, 431, 210
 Chiaberge M., Marconi A., 2011, *MNRAS*, 416, 917
 Chiar J. E., Tielens A. G. G. M., 2006, *ApJ*, 637, 774
 Collin S., Kawaguchi T., 2004, *A&A*, 426, 797
 Collin S., Kawaguchi T., Peterson B., Vestergaard M., 2006, *A&A*, 456, 75
 Condon J. J., Cotton W. D., Broderick J. J., 2002, *AJ*, 124, 675
 Condon J. J., Cotton W. D., Greisen E. W., Yin Q. F., Perley R. A., Taylor G. B., Broderick J. J., 1998, *AJ*, 115, 1693
 Cotton W. D. et al., 2003, *PASA*, 20, 12
 Dallacasa D., Fanti C., Fanti R., Schilizzi R. T., Spencer R. E., 1995, *A&A*, 295, 27
 Dallacasa D., Orienti M., Fanti C., Fanti R., Stanghellini C., 2013, *MNRAS*, 433, 147
 Decarli R., Dotti M., Fontana M., Haardt F., 2008, *MNRAS*, 386, L15
 Denney K. D., Peterson B. M., Dietrich M., Vestergaard M., Bentz M. C., 2009, *ApJ*, 692, 246
 Deo R. P., Crenshaw D. M., Kraemer S. B., 2006, *AJ*, 132, 321
 Doi A., Asada K., Fujisawa K., Nagai H., Hagiwara Y., Wajima K., Inoue M., 2013, *ApJ*, 765, 69
 Doi A., Nagira H., Kawakatu N., Kino M., Nagai H., Asada K., 2012, *ApJ*, 760, 41
 Domínguez A. et al., 2013, *ApJ*, 763, 145
 Donato D., Ghisellini G., Tagliaferri G., Fossati G., 2001, *A&A*, 375, 739
 Fabian A. C., Miniutti G., Gallo L., Boller T., Tanaka Y., Vaughan S., Ross R. R., 2004, *MNRAS*, 353, 1071
 Fanali R., Caccianiga A., Severgnini P., Della Ceca R., Marchese E., Carrera F. J., Corral A., Mateos S., 2013, *MNRAS*, 433, 648
 Fanti C., Pozzi F., Dallacasa D., Fanti R., Gregorini L., Stanghellini C., Vigotti M., 2001, *A&A*, 369, 380
 Fanti R., Fanti C., Schilizzi R. T., Spencer R. E., Nan Rendong, Parma P., van Breugel W. J. M., Venturi T., 1990, *A&A*, 231, 333
 Foschini L., 2011, *Proceedings of Science (PoS, Trieste, Italy)*, vol. NLS1, Published online at <http://pos.sissa.it/cgi-bin/reader/conf.cgi?confid=126>, id.24
 Foschini L., 2012, in *High energy gamma-ray astronomy: 5th International Meeting on High Energy Gamma-Ray Astronomy*. AIP Conference Proceedings, Vol. 1505, pp. 574–577
 Foschini L., 2013, *Proceedings of Science (PoS, Trieste, Italy)*, vol. Seyfert2012, Published on-line at <http://pos.sissa.it/cgi-bin/reader/conf.cgi?confid=169>, id.10
 Foschini L. et al., 2012, *A&A*, 548, A106
 Foschini L., Fermi/Lat Collaboration, Ghisellini G., Maraschi L., Tavecchio F., Angelakis E., 2010, “Accretion and Ejection in AGN: A Global View”, *ASP Conference Series*, 427, 243
 Gallo L. C., 2006, *MNRAS*, 368, 479
 Gallo L. C. et al., 2006, *MNRAS*, 370, 245
 Gaskell C. M., Ferland G. J., 1984, *PASP*, 96, 393
 Gelderman R., Whittle M., 1994, *ApJS*, 91, 491
 Goodrich R. W., 1989, *ApJ*, 342, 224
 Greene J. E., Ho L. C., 2004, *ApJ*, 610, 722
 Greene J. E., Ho L. C., 2005, *ApJ*, 627, 721
 Gregory P. C., Scott W. K., Douglas K., Condon J. J., 1996, *ApJS*, 103, 427
 Grupe D., 2004, *AJ*, 127, 1799
 Grupe D., Komossa S., Gallo L. C., Longinotti A. L., Fabian A. C., Pradhan A. K., Gruberbauer M., Xu D., 2012, *ApJS*, 199, 28
 Grupe D., Komossa S., Leighly K. M., Page K. L., 2010, *ApJS*, 187, 64
 Grupe D., Mathur S., 2004, *ApJ*, 606, L41
 Gültekin K. et al., 2009, *ApJ*, 698, 198
 Haardt F., Maraschi L., 1991, *ApJ*, 380, L51
 Hales S. E. G., Riley J. M., Waldram E. M., Warner P. J., Baldwin

- J. E., 2007, MNRAS, 382, 1639
- Hamilton T. S., Foschini L., 2012, AAS, 220
- Holt J., Tadhunter C. N., Morganti R., 2008, MNRAS, 387, 639
- Ibar E. et al., 2013, MNRAS, 434, 3218
- Jester S. et al., 2005, ApJ, 130, 873
- Kellermann K., Sramek R., Schmidt M., Shaffer D., Green R., 1989, AJ, 98, 1195
- Kennicutt R. C., 1998, ARA&A, 36, 189
- Kim M., Ho L. C., Lonsdale C. J., Lacy M., Blain A. W., Kimball A. E., 2013, ApJ, 768, L9
- Komossa S., Voges W., Xu D., Mathur S., Adorf H.-M., Lemson G., Duschl W. J., Grupe D., 2006, AJ, 132, 531
- Komossa S., Xu D., 2007, ApJ, 667, L33
- Komossa S., Xu D., Zhou H., Storchi-Bergmann T., Binette L., 2008, ApJ, 680, 926
- Lacy M., Laurent-Muehleisen S., Ridgway S., Becker R., White R., 2001, ApJ, 551, L17
- Lane W. M., Cotton W. D., Helmboldt J. F., Kassim N. E., 2012, Radio Science, 47, RS0K04
- Maiolino R., Marconi A., Salvati M., Risaliti G., Severgnini P., Oliva E., La Franca F., Vanzi L., 2001, A&A, 365, 28
- Marconi A., Axon D. J., Maiolino R., Nagao T., Pastorini G., Pietrini P., Robinson A., Torricelli G., 2008, ApJ, 678, 693
- Marconi A., Risaliti G., Gilli R., Hunt L. K., Maiolino R., Salvati M., 2004, MNRAS, 351, 169
- Marziani P., Sulentic J. W., Zwitter T., Dultzin-Hacyan D., Calvani M., 2001, ApJ, 558, 553
- Marziani P., Zamanov R. K., Sulentic J. W., Calvani M., 2003, MNRAS, 345, 1133
- Mattox J. R. et al., 1996, ApJ, 461, 396
- Migliori G., Siemiginowska A., Kelly B. C., Stawarz L., Celotti A., Begelman M. C., 2013, ApJ, in press
- Moran E. C., 2000, New Astronomy Reviews, 44, 527
- Murgia M., 2003, PASA, 20, 19
- Murgia M., Fanti C., Fanti R., Gregorini L., Klein U., Mack K.-H., Vigotti M., 1999, A&A
- Nesvadba N. P. H., Polletta M., Lehnert M. D., Bergeron J., De Breuck C., Lagache G., Omont A., 2011, MNRAS, 415, 2359
- Netzer H., 2009, ApJ, 695, 793
- Nolan P. L. et al., 2012, ApJS, 199, 31
- O'Dea C. P., 1998, PASP, 110, 493
- Oshlack A. Y. K. N., Webster R. L., Whiting M. T., 2001, ApJ, 558, 578
- Osterbrock D. E., Pogge R. W., 1985, ApJ, 297, 166
- Park D. et al., 2012, ApJ, 747, 30
- Peng C. Y., Ho L. C., Impey C. D., Rix H.-W., 2002, AJ, 124, 266
- Peng C. Y., Ho L. C., Impey C. D., Rix H.-W., 2010, AJ, 139, 2097
- Pogge R. W., 2000, New Astronomy Reviews, 44, 381
- Pogge R. W., 2011, Proceedings of Science (PoS, Trieste, Italy), vol. NLS1, Published online at <http://pos.sissa.it/cgi-bin/reader/conf.cgi?confid=126>, id.2
- Polatidis A. G., Conway J. E., 2003, PASA, 20, 69
- Polletta M. et al., 2007, ApJ, 663, 81
- Pozo Nuñez F. et al., 2013, A&A, 552, A1
- Rengelink R. B., Tang Y., de Bruyn A. G., Miley G. K., Bremer M. N., Rttgering H. J., Bremer M. A., 1997, A&AS, 124, 259
- Richards G. T. et al., 2006, ApJS, 166, 470
- Sanders D. B., Mirabel I. F., 1996, ARA&A, 34, 749
- Sani E. et al., 2012, MNRAS, 424, 1963
- Sani E., Lutz D., Risaliti G., Netzer H., Gallo L. C., Trakhtenbrot B., Sturm E., Boller T., 2010, MNRAS, 403, 1246
- Shen Y. et al., 2011, ApJS, 194, 45
- Siemiginowska A., 2009, AN, 330, 264
- Sikora M., 2009, AN, 330, 291
- Sikora M., Stawarz L., Lasota J.-P., 2007, ApJ, 658, 815
- Sulentic J. W., Marziani P., Dultzin-Hacyan D., 2000, ARA&A, 38, 521
- Tanaka Y., Boller T., Gallo L., Keil R., Ueda Y., 2004, PASJ
- Taylor G. B., Vermeulen R. C., Readhead A. C. S., Pearson T. J., Henstock D. R., Wilkinson P. N., 1996, ApJS, 107, 37
- Urry C. M., Padovani P., 1995, PASP, 107, 803
- Véron-Cetty M.-P., Joly M., Véron P., 2004, A&A, 417, 515
- Véron-Cetty M.-P., Véron P., Gonçalves A. C., 2001, A&A, 372, 730
- Vestergaard M., Peterson B. M., 2006, ApJ, 641, 689
- Voges W. et al., 1999, A&A
- Volonteri M., Sikora M., Lasota J.-p., 2007, ApJ, 667, 704
- Warwick R. S., Saxton R. D., Read A. M., 2012, A&A, 548, A99
- Whalen D. J., Laurent-Muehleisen S. a., Moran E. C., Becker R. H., 2006, AJ, 131, 1948
- Wright E. L. et al., 2010, AJ, 140, 1868
- Yuan W., Zhou H. Y., Komossa S., Dong X. B., Wang T. G., Lu H. L., Bai J. M., 2008, ApJ, 685, 801
- Zhou H., Wang T., Yuan W., Lu H., Dong X., Wang J., Lu Y., 2006, ApJS, 166, 128
- Zhou H. et al., 2007, ApJ, 658, L13
- Zhou X.-L., Zhang S.-N., 2010, ApJ, 713, L11